Small signal modeling of restructured boost converter in continuous conduction mode

Anwar Muqorobin, Sulistyo Wijanarko, Muhammad Kasim, Pudji Irasari, Ketut Wirtayasa, Puji Widiyanto
Research Center for Energy Conversion and Conservation, National Research and Innovation Agency, KST Samaun Samadikun, Bandung, Indonesia

Article Info

Article history:

Received Apr 15, 2025
Revised Aug 22, 2025
Accepted Sep 2, 2025

Keywords:

Circuit averaging
Continuous conduction mode
Conventional boost converter
Restructured boost converter
Small signal model

ABSTRACT

This paper introduces small signal modeling of the restructured boost converter (RBC) in continuous conduction mode (CCM) by using the circuit averaging technique. The averaging technique produces linear transfer functions of the converter. The transfer functions relating the duty cycle to output voltage, duty cycle to inductor current, input voltage to output voltage, and input voltage to inductor current are obtained. To validate the converter model, power simulation (PSIM) simulations are developed, and experiments are conducted. The function of RBC is similar to a conventional boost converter, i.e., to level up the input voltage. A comparative analysis between the RBC and conventional boost converter is performed. The results highlight the advantages of RBC over a conventional boost converter.

Corresponding Author:

Anwar Muqorobin
Research Center for Energy Conversion and Conservation, National Research and Innovation Agency
KST Samaun Samadikun
Bandung, Indonesia
Email: anwa014@brin.go.id

1. INTRODUCTION

For remote areas, microgrid or standalone generation is needed due to the lack of distribution infrastructure from the main power system. In this case, renewable energy sources are a suitable solution. Renewable energy, especially photovoltaic, produces low-level voltage. In most applications, this low voltage is mandatory to be stepped up, which is commonly done by a boost converter. A conventional boost converter has a low input current ripple that is suitable for photovoltaic applications. The other applications that use a step-up converter are battery charging/discharging and a pico-hydro power system. In an AC motor drive, a step-up converter is used because a high-voltage DC link allows a linear modulation index range can be used in the inverter to produce low harmonic output current.

A new converter has been proposed in [1]-[4]. The converter has a function to level up the input voltage, similar to a conventional boost converter. The converter topology is obtained by rearranging the components of the conventional boost converter, i.e., by shifting the negative terminal of the output capacitor from the common ground to the input positive terminal. The resulting converter is named as restructured boost converter (RBC) [1]. This converter can also be obtained from the buck-boost converter topology [2]. Although the efficiency of RBC is only slightly higher than that of a conventional boost converter, the main benefit is less voltage stress on the output capacitor. The capacitor failure rate is a cubic function of the ratio of the operating voltage to the rated voltage. Therefore, by using capacitors with a similar voltage rating, RBC offers a longer lifetime expectation compared to a conventional boost converter. RBC has been used in [3], [4] as part of a semi-two-stage photovoltaic inverter, which gives higher efficiency compared to a two-stage inverter topology. The DC-DC converter is operated when the photovoltaic voltage is lower than the grid voltage.

To regulate the output voltage under various conditions (load, input voltage, and converter components variations), a pulse width modulation (PWM) converter needs a control circuit. The control is built upon the model of the converter. A PWM converter contains passive and active components. The passive components can be an inductor and a capacitor, and the active components are a transistor and a diode. The active components are used as a switch, which is activated by a PWM signal. The PWM signal has two conditions, i.e., ON and OFF. To produce a single equation model, the averaging technique is used. We already know two averaging techniques, i.e., state space averaging and circuit averaging techniques. State space averaging produces a linear equation for the buck converter and nonlinear equations for boost and buck-boost converters. Linearization is needed for the last two converters if linear control is used. State space averaging has been used to design modern control, e.g., adaptive control, dynamic evolution control, linear quadratic regulator (LQR) control, active disturbance rejection control, feedback linearization, sliding mode control, and fuzzy logic control [5]-[15]. Circuit averaging produces a linear transfer function that can be used to design linear control, such as proportional integral derivative (PID), pole placement, and lead-lag controls. In circuit averaging, we will get the linear equation directly for all converters. Compared to state space averaging, circuit averaging is relatively simple and gives an easy understanding of the converter behavior. This method has been used to model buck, boost, buck-boost, SEPIC, Cuk, and impedance source converters [16]-[24] by modeling the transistor as a current-dependent current source and the diode as a voltage-dependent voltage source. Circuit averaging gives transfer functions of duty cycle to output voltage and inductor current, transfer functions of input voltage to output voltage and inductor current, and input and output impedances. In this paper, the RBC model in continuous conduction mode (CCM) is proposed. The model is based on the circuit averaging technique. Comparison to a conventional boost converter is presented. Power simulation (PSIM) simulations and laboratory experiments are used to clarify the converter modeling.

2. SMALL-SIGNAL MODELING OF RBC

The circuits of the conventional boost converter and RBC are shown in Figures 1(a) and 1(b), respectively. Both converters are almost similar and use similar components, i.e. transistor S, diode D_i, inductor L, and capacitor C. The transistor, diode, and inductor are connected in a similar configuration. The difference is that the negative terminal of the RBC output capacitor is connected to the positive terminal of the input, not to the negative one, as in a boost converter. Practically, all components are ideal. The non-idealities are represented by inductor equivalent series resistance (ESR) r_L, capacitor ESR r_C, diode forward resistance R_F, and the transistor on resistance r_{ON}.

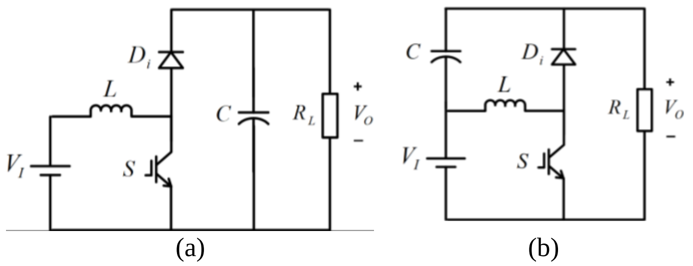

Figure 1. The circuits of: (a) a conventional boost converter and (b) RBC

Figures 2(a) and 2(b) represent the small signal models of a conventional boost converter in CCM operation and RBC, respectively. Here, V_O and v_o are the DC and AC elements of the output voltage, and V_i and v_i are the DC and AC elements of the input voltage, respectively; I_L and i_l are the DC and AC parts of the inductor current, and i_o is the AC element of the output current; D and d are the DC and AC elements of the on-duty cycle of the switch; and R_L is the load resistance. To get the transfer functions of the duty cycle to the output voltage $v_o(s)/d\,(s)$ and the duty cycle to the inductor current $i_L(s)/d(s)$, we set $v_i = 0$ and $i_o = 0$. Then the circuits in Figures 2(a) and 2(b) will produce a similar circuit as shown in Figure 3, and the resulting transfer functions become similar. Because of this, we can implement the control of a conventional boost converter to RBC directly. From [25] we get:

$$T_p(s) = \left.\frac{v_o(s)}{d(s)}\right|_{v_i=i_o=0} = T_{po}\frac{\left(1+\frac{s}{\omega_{zn}}\right)\left(1-\frac{s}{\omega_{zp}}\right)}{1+\frac{2\xi}{\omega_0}s+\left(\frac{s}{\omega_0}\right)^2} \quad (1)$$

where:

$$T_{po} = \frac{V_O}{1-D}\frac{R_L(1-D)^2-r}{R_L(1-D)^2+r} \tag{2}$$

$$\omega_0 = \sqrt{\frac{(1-D)^2R_L+r}{LC(R_L+r_C)}} \tag{3}$$

$$\xi = \frac{L+C[r(R_L+r_C)+(1-D)^2R_Lr_C]}{2\sqrt{LC(R_L+r_C)[(1-D)^2R_L+r]}} \tag{4}$$

$$\omega_{zn} = \frac{1}{Cr_c} \tag{5}$$

$$\omega_{zp} = \frac{R_L(1-D)^2-r}{L} \tag{6}$$

$$r = Dr_{ON} + (1-D)R_F + r_L \tag{7}$$

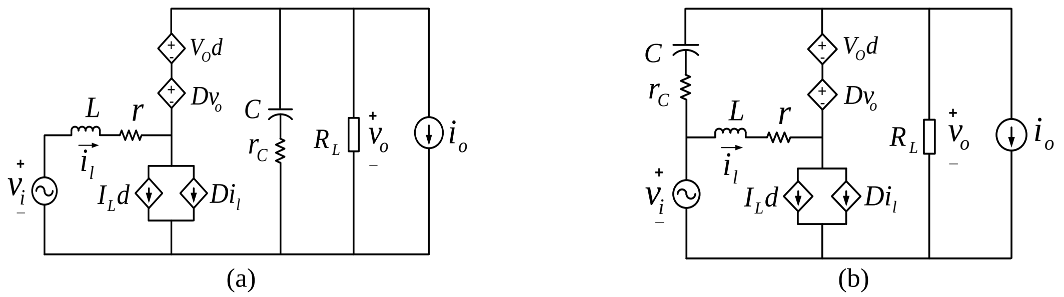

Figure 2. Small signal models of (a) CCM boost converter and (b) CCM RBC

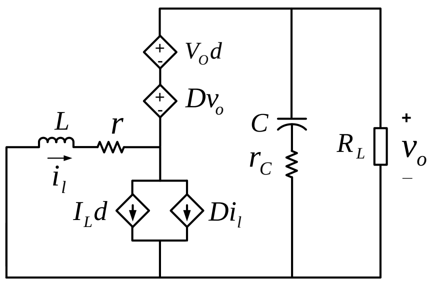

Figure 3. Small-signal model for RBC and conventional boost converter to determine the transfer functions of duty cycle to output voltage and inductor current

The transfer function of duty cycle to inductor current is (8):

$$T_{pi}(s) = \left.\frac{i_i(s)}{d(s)}\right|_{v_i=i_o=0} = T_{pio}\frac{\left(1+\frac{s}{\omega_{zi}}\right)}{1+\frac{2\xi}{\omega_0}s+\left(\frac{s}{\omega_0}\right)^2} \tag{8}$$

where:

$$T_{pio} = \frac{2V_O}{(1-D)^2R_L+r} \tag{9}$$

$$\omega_{zi} = \frac{1}{C(R_L/2+r_C)} \tag{10}$$

By setting $d = 0$ and $i_o = 0$ we get the circuits for boost converter and RBC as displayed in Figures 4(a) and 4(b), respectively. The input voltage to output voltage transfer function of conventional boost converter is (11):

$$M_v(s) = \frac{v_o(s)}{v_i(s)}\Big|_{d=i_o=0} = M_{vo}\frac{\left(1+\frac{s}{\omega_{znb}}\right)}{1+\frac{2\xi}{\omega_0}s+\left(\frac{s}{\omega_0}\right)^2} \tag{11}$$

where

$$M_{vo} = \frac{(1-D)R_L}{R_L(1-D)^2+r} \tag{12}$$

$$\omega_{znb} = \frac{1}{Cr_c} \tag{13}$$

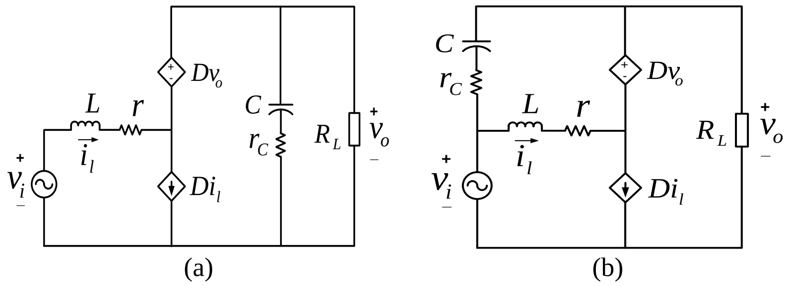

Figure 4. Small-signal models to determine the transfer function of input voltage to output voltage and inductor current: (a) conventional boost converter and (b) RBC

The transfer function of input voltage to output voltage for RBC is:

$$M_v(s) = \frac{v_o(s)}{v_i(s)}\Big|_{d=i_o=0} = M_{vo}\frac{1+s\frac{rC+r_C C(1-D)}{1-D}+s^2\frac{LC}{1-D}}{1+\frac{2\xi}{\omega_0}s+\left(\frac{s}{\omega_0}\right)^2} \tag{14}$$

The transfer function of input voltage to inductor current for conventional boost converter is:

$$M_{vi}(s) = \frac{i_l(s)}{v_i(s)}\Big|_{d=i_o=0} = M_{vio}\frac{\left(1+\frac{s}{\omega_{zib}}\right)}{1+\frac{2\xi}{\omega_0}s+\left(\frac{s}{\omega_0}\right)^2} \tag{15}$$

where

$$M_{vio} = \frac{1}{(1-D)^2R_L+r} \tag{16}$$

$$\omega_{zib} = \frac{1}{C(R_L+r_C)} \tag{17}$$

In the case of the RBC, the transfer function related to input voltage to inductor current is given by:

$$M_{vi}(s) = \frac{i_l(s)}{v_i(s)}\Big|_{d=i_o=0} = M_{vio}\frac{\left(1+\frac{s}{\omega_{zim}}\right)}{1+\frac{2\xi}{\omega_0}s+\left(\frac{s}{\omega_0}\right)^2} \tag{18}$$

$$\omega_{zim} = \frac{1}{C(DR_L+r_C)} \tag{19}$$

From (15) and (18), we know that the transfer functions of input voltage to inductor current of the conventional boost converter and RBC have a similar characteristic equation. However, the difference can be seen at the zero location. The zero of the boost converter is located closer to the imaginary axis compared to the zero of RBC. As a result, the response of the boost converter has a higher overshoot than RBC.

Additionally, from (11) and (14), it can be observed that the boost converter and the RBC exhibit similar magnitude in their input-to-output voltage transfer functions, denoted as M_{vo}. Likewise, (15) and (18) indicate that the magnitude of the transfer function of input voltage to inductor current M_{vio}, is also similar. It implies that both converters exhibit similar output voltage and inductor current steady state responses to input voltage variations. However, their transient responses differ due to the difference in zero locations.

3. RESULTS AND DISCUSSION

To clarify the converter models, we conduct PSIM simulations and laboratory experiments. Figure 5 shows the experimental setup. The converter is made of an inductor L of 2.1 mH, inductor ESR r_L of 0.5 Ohm, a capacitor C of 47 uF, capacitor ESR r_C of 0.5 Ohm, IGBT FGL40N120AND with $r_{ON} = 0.2$ Ohm, diode forward resistance R_F of 0.5 Ohm. The load resistance is 200 Ohms and the input voltage is 48 volts. The duty cycle is programmed in the digital signal processor (DSP) TMS320F28379D from Texas Instruments. The switching frequency is 10 kHz. The inductor current is sensed by the ACS712 current sensor, and the input and output voltages by the Hantek differential probe HT8050.

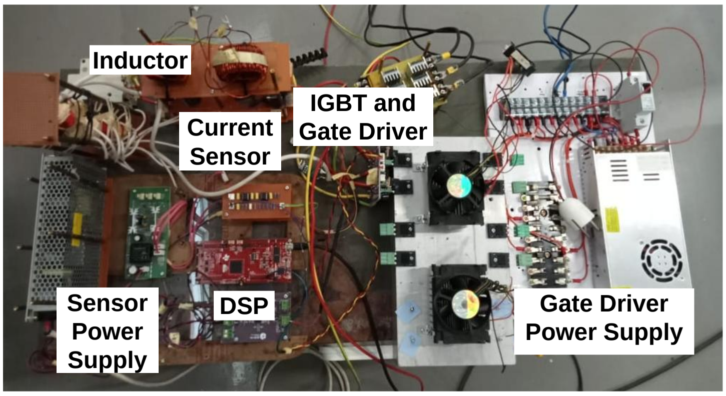

Figure 5. Experimental setup

The output voltage and inductor current responses to a step change in the duty cycle are depicted in Figure 6, where the duty cycle is changed from 0.6 to 0.65. The comparison of the converter model in (1) and (8) to the experimental results shows that the agreement between them can be appreciated, as shown in Figure 7, with Figure 7(a) for the output voltage and Figure 7(b) for the inductor current. Figure 8 presents the output responses to a step change in input voltage from 48 V to 58 V, for the output voltage and inductor current in parts Figures 8(a) and 8(b), respectively. The plots reveal that the RBC has lower overshoot than the boost converter, which is consistent with the prediction in the previous section. The PSIM simulation results depicted in Figure 9, where Figure 9(a) presents the output voltage and Figure 9(b) displays the inductor current, further reinforce this finding, confirming the model's accuracy.

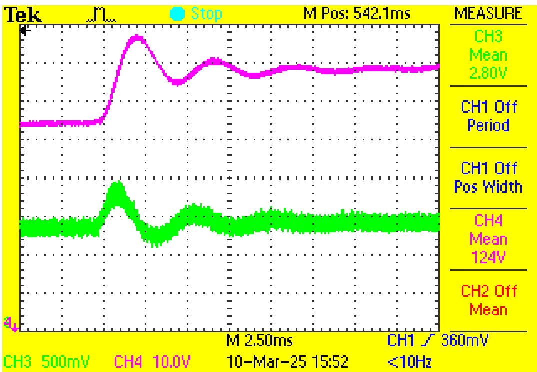

Figure 6. The responses of the output voltage (upper signal) and the inductor current (lower signal) to duty cycle step change

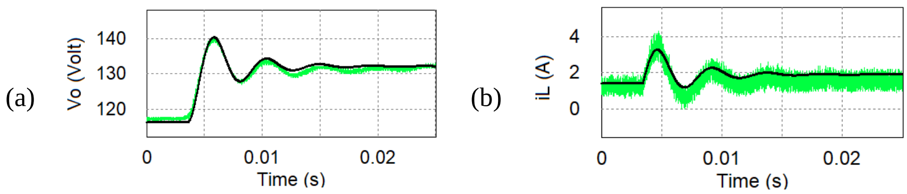

Figure 7. Output responses to duty cycle step change (black trace: converter model and green trace: experimental result): (a) output voltage and (b) inductor current

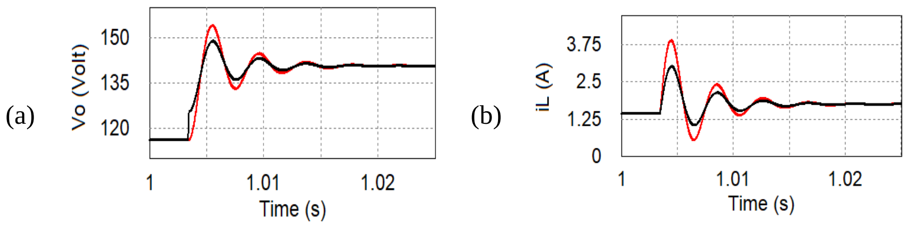

Figure 8. The output responses to the input voltage step change of the boost converter (red trace) and RBC (black trace): (a) output voltage and (b) inductor current

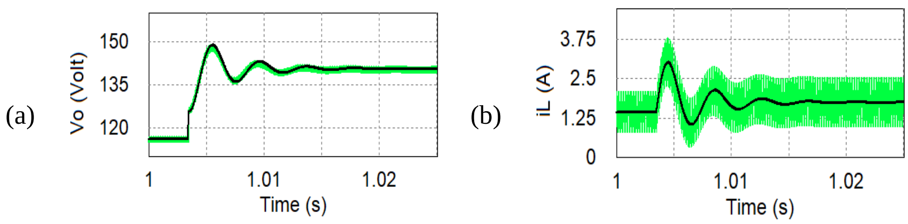

Figure 9. The output responses to the input voltage step change (black trace: converter model and green trace: simulation): (a) output voltage and (b) inductor current

Figure 10 exhibits the experimental results of the converter responses to variation in input voltage. The input voltage in this case is obtained from a three-phase source and rectifier without an output filter. The respective input voltage signal and the inductor current are shown in Figure 10(a), and their associated output voltage response is shown in Figure 10(b). Figure 11 presents a comparison between the experimental results and the converter model, with part (a) showing the output voltage and part (b) showing the inductor current. However, we can see a discrepancy in Figure 11(a) because in the experiment, the used switching frequency is not so high with respect to the input frequency.

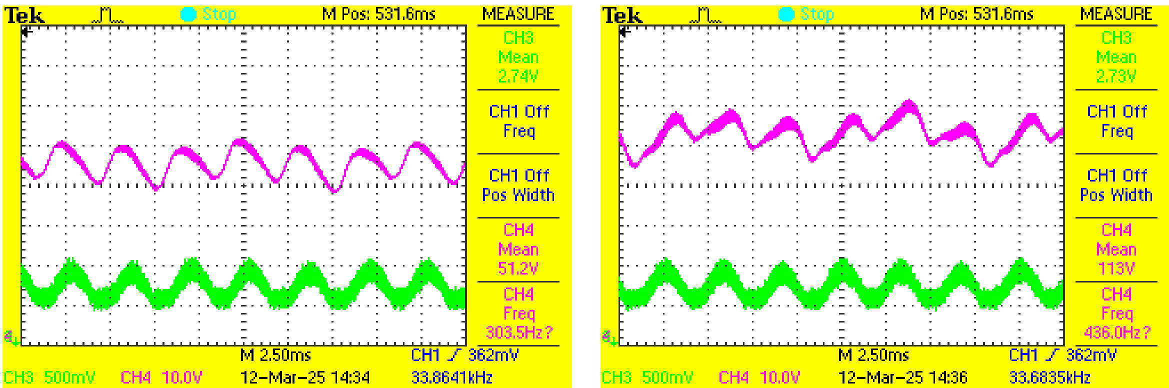

(a) (b)

Figure 10. RBC output responses to input voltage variation: (a) input voltage (upper signal) and inductor current (lower signal) (b) output voltage (upper signal) and inductor current (lower signal)

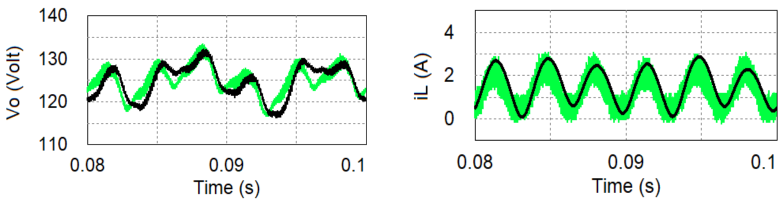

(a) (b)

Figure 11. RBC output responses from converter model (black trace) and experimental result (green trace): (a) output voltage and (b) inductor current

4. CONCLUSION

Circuit averaging technique has been used to obtain the transfer functions of duty cycle to output voltage and inductor current and input voltage to output voltage and inductor current of RBC. The RBC transfer functions of duty cycle to output voltage and inductor current are similar to standard boost converter. Therefore, RBC can adopt similar control design to that of standard boost converter. In comparison to standard boost converter, the RBC transfer functions of input voltage to output voltage and inductor current exhibit reduced overshoot. However, the steady-state responses of the RBC are similar to those of standard boost converter.

FUNDING INFORMATION

This work is supported by Rumah Program Energi Berkelanjutan number 7/III.3/HK/2025, Research Organization for Energy and Manufacture, National Research and Innovation Agency (BRIN).

AUTHOR CONTRIBUTIONS STATEMENT

This journal uses the Contributor Roles Taxonomy (CRediT) to recognize individual author contributions, reduce authorship disputes, and facilitate collaboration.

Name of Author	C	M	So	Va	Fo	I	R	D	O	E	Vi	Su	P	Fu
Anwar Muqorobin	✓	✓		✓	✓	✓		✓	✓					
Sulistyo Wijanarko	✓	✓	✓		✓		✓	✓	✓					
Muhammad Kasim				✓		✓				✓	✓			
Pudji Irasari					✓	✓			✓	✓				
Ketut Wirtayasa		✓		✓		✓	✓			✓				
Puji Widiyanto		✓	✓				✓	✓		✓				

C : **C**onceptualization
M : **M**ethodology
So : **So**ftware
Va : **Va**lidation
Fo : **Fo**rmal analysis
I : **I**nvestigation
R : **R**esources
D : **D**ata Curation
O : Writing -**O**riginal Draft
E : Writing - Review &**E**diting
Vi : **Vi**sualization
Su : **Su**pervision
P : **P**roject administration
Fu : **Fu**nding acquisition

CONFLICT OF INTEREST STATEMENT

Authors state no conflict of interest.

DATA AVAILABILITY

The authors confirm that the data supporting the findings of this study are available within the article [and/or its supplementary materials].

REFERENCES

[1] M. J. Sathik, J. D. Navamani, A. Lavanya, Y. Yang, D. Almakhles, and F. Blaabjerg, "Reliability analysis of power components in restructured dc/dc converters," *IEEE Transactions on Device and Materials Reliability*, vol. 21, no. 4, pp. 544–555, 2021, doi: 10.1109/TDMR.2021.3116941.

[2] R. D. N. Aditama, N. Ramadhani, J. Furqani, A. Rizqiawan, and P. A. Dahono, "New bidirectional step-up DC-DC converter derived from buck-boost dc-dc converter," *International Journal of Power Electronics and Drive Systems*, vol. 12, no. 3, pp. 1699–1707, 2021, doi: 10.11591/ijpeds.v12.i3.pp1699-1707.
[3] L. Zhang, F. Jiang, D. D. Xu, K. Sun, Y. Hao, and T. Zhang, "Two-stage transformer-less dual-buck PV grid-connected inverters with high efficiency," *Chinese Journal of Electrical Engineering*, vol. 4, no. 2, pp. 36–42, 2018, doi: 10.23919/CJEE.2018.8409348.
[4] A. Anurag, N. Deshmukh, A. Maguluri, and S. Anand, "Integrated DC-DC converter-based grid-connected transformer-less photovoltaic inverter with extended input voltage range," *IEEE Transactions on Power Electronics*, vol. 33, no. 10, pp. 8322–8330, 2018, doi: 10.1109/TPEL.2017.2779144.
[5] C. Yanarates and Z. Zhou, "Design and cascade pi controller-based robust model reference adaptive control of DC-DC boost converter," *IEEE Access*, vol. 10, pp. 44909–44922, 2022, doi: 10.1109/ACCESS.2022.3169591.
[6] A. S. Samosir, S. R. Sulistiyanti, H. Gusmedi, and L. Mardiyah, "Dynamic evolution control for the DC/DC boost converter design and implementation," *International Journal of Power Electronics and Drive Systems (IJPEDS)*, vol. 15, no. 1, pp. 357–366, 2024, doi: 10.11591/ijpeds.v15.i1.pp357-366.
[7] H. B. Yuan and Y. B. Kim, "Compensated active disturbance rejection control for voltage regulation of a DC–DC boost converter," *IET Power Electronics*, vol. 14, no. 2, pp. 432–441, 2021, doi: 10.1049/pel2.12049.
[8] J. Sun, J. Xia, S. Ding, and X. Yu, "Exact-feedback-linearization-based adaptive second-order sliding mode control design for DC–DC boost converters," *IEEE Transactions on Industrial Electronics*, vol. 72, no. 5, pp. 5397–5407, 2025, doi: 10.1109/TIE.2024.3476994.
[9] Q. Guo, M. J. Carrizosa, A. Iovine, and A. Arzande, "Dynamic feedback linearization and singular perturbation for a stabilizing controller for dc/dc boost converters: theory and experimental validation," *IEEE Transactions on Industrial Electronics*, vol. 71, no. 8, pp. 9559–9568, 2024, doi: 10.1109/TIE.2023.3312425.
[10] D. O. Neacsu and A. Sirbu, "Design of a LQR-Based boost converter controller for energy savings," *IEEE Transactions on Industrial Electronics*, vol. 67, no. 7, pp. 5379–5388, Jul. 2020, doi: 10.1109/TIE.2019.2934062.
[11] S. Ahmad and A. Ali, "Unified disturbance-estimation-based control and equivalence with IMC and PID: case study on a DC-DC boost converter," *IEEE Transactions on Industrial Electronics*, vol. 68, no. 6, pp. 5122–5132, 2021, doi: 10.1109/TIE.2020.2987269.
[12] Y. Wang, Y. Wang, X. Song, and Z. Liang, "Finite-Time adaptive neural network observer-based output voltage-tracking control for DC–DC boost converters," *IEEE Transactions on Circuits and Systems I: Regular Papers*, vol. 70, no. 7, pp. 3005–3016, Jul. 2023, doi: 10.1109/TCSI.2023.3264536.
[13] J. Wang, W. Luo, J. Liu, and L. Wu, "Adaptive Type-2 FNN-Based dynamic sliding mode control of DC–DC boost converters," *IEEE Transactions on Systems, Man, and Cybernetics: Systems*, vol. 51, no. 4, pp. 2246–2257, Apr. 2021, doi: 10.1109/TSMC.2019.2911721.
[14] N. Agrawal, S. Samanta, and S. Ghosh, "Modified LQR technique for fuel-cell-integrated boost converter," *IEEE Transactions on Industrial Electronics*, vol. 68, no. 7, pp. 5887–5896, Jul. 2021, doi: 10.1109/TIE.2020.3000096.
[15] H. Al-Baidhani, T. Salvatierra, R. Ordonez, and M. K. Kazimierczuk, "Simplified nonlinear voltage-mode control of PWM DC-DC buck converter," *IEEE Transactions on Energy Conversion*, vol. 36, no. 1, pp. 431–440, 2021, doi: 10.1109/TEC.2020.3007739.
[16] A. Ayachit and M. K. Kazimierczuk, "Averaged small-signal model of PWM DC-DC converters in CCM including switching power loss," *IEEE Transactions on Circuits and Systems II: Express Briefs*, vol. 66, no. 2, pp. 262–266, 2019, doi: 10.1109/TCSII.2018.2848623.
[17] A. Chadha and M. K. Kazimierczuk, "Small-signal modelling of open-loop PWM tapped-inductor buck DC-DC converter in ccm," *IEEE Transactions on Industrial Electronics*, vol. 68, no. 7, pp. 5765–5775, 2021, doi: 10.1109/TIE.2020.2996157.
[18] A. Ayachit, Y. P. Siwakoti, V. P. N. Galigekere, M. K. Kazimierczuk, and F. Blaabjerg, "Steady-state and small-signal analysis of a-source converter," *IEEE Transactions on Power Electronics*, vol. 33, no. 8, pp. 7118–7131, 2018, doi: 10.1109/TPEL.2017.2756626.
[19] L. Kathi, A. Ayachit, D. K. Saini, A. Chadha, and M. K. Kazimierczuk, "Open-loop small-signal modelling of cuk DC-DC converter in CCM by circuit-averaging technique," in *2018 IEEE Texas Power and Energy Conference, TPEC 2018*, 2018, pp. 1–6. doi: 10.1109/TPEC.2018.8312045.
[20] A. Ayachit, A. Reatti, and M. K. Kazimierczuk, "Small-signal modeling of PWM dual-sepic DC-DC converter by circuit averaging technique," in *IECON Proceedings (Industrial Electronics Conference)*, 2016, pp. 3606–3611. doi: 10.1109/IECON.2016.7793030.
[21] M. Bartoli, A. Reatti, and M. K. Kazimierczuk, "Open loop small-signal control-to-output transfer function of pwm buck converter for CCM: modeling and measurements," in *Proceedings of the Mediterranean Electrotechnical Conference - MELECON*, 1996, pp. 1203–1206. doi: 10.1109/melcon.1996.551161.
[22] A. Reatti and M. K. Kazimierczuk, "Small-signal model of pwm converters for discontinuous conduction mode and its application for boost converter," *IEEE Transactions on Circuits and Systems I: Fundamental Theory and Applications*, vol. 50, no. 1, pp. 65–73, 2003, doi: 10.1109/TCSI.2002.805709.
[23] D. K. Saini and M. K. Kazimierczuk, "Open-loop transfer functions of buck-boost converter by circuit-averaging technique," *IET Power Electronics*, vol. 12, no. 11, pp. 2858–2864, 2019, doi: 10.1049/iet-pel.2018.5514.
[24] B. Bryant and M. K. Kazimierczuk, "Voltage-loop power-stage transfer functions with MOSFET delay for boost PWM converter operating in CCM," *IEEE Transactions on Industrial Electronics*, vol. 54, no. 1, pp. 347–353, 2007, doi: 10.1109/TIE.2006.885136.
[25] M. K. Kazimierczuk, *Pulse-width modulated DC–DC power converters*, 2nd ed. John Wiley & Sons, Ltd, 2016.

BIOGRAPHIES OF AUTHORS

Anwar Muqorobin studied electrical engineering at Diponegoro University and Bandung Institute of Technology. At present, he is a researcher at National Research and Innovation Agency (BRIN). His research activities are focused on DC-DC converters, inverters, and control applications. He can be contacted at email: anwa014@brin.go.id.

Sulistyo Wijanarko received his bachelor's degree in Electrical Engineering from Gadjah Mada University in 2013 and his master's degree from Bandung Institute of Technology in 2021. At present, he is a research assistant at the National Research and Innovation Agency (BRIN), Indonesia. His field of research is power electronics and drives. He can be contacted at email: sulistyo.wijanarko@brin.go.id.

Muhammad Kasim is a researcher at the Research Center for Energy Conversion and Conservation, National Research and Innovation Agency (BRIN), Indonesia. He received his bachelor's degree in electrical engineering from Hasanuddin University in 2003 and his master's degree in renewable energy from Murdoch University in 2014. He finished his Ph.D. in Electrical Engineering at the School of Electrical Engineering and Telecommunications, University of New South Wales in 2022. His research interests include electrical machines and renewable energy management systems. He can be contacted at email: muha087@brin.go.id.

Pudji Irasari is a researcher at the Research Center for Energy Conversion and Conservation, National Research and Innovation Agency (BRIN), Indonesia. She received her bachelor's degree in electrical engineering from Brawijaya University in 1994 and her master's degree in renewable energy from Oldenburg University in 2003. Her research interests include electrical machines (motors and generators) and renewable energy-based power generation, particularly wind, water, and ocean energy. She can be contacted at email: pudj003@brin.go.id.

Ketut Wirtayasa is a researcher at the Research Center for Energy Conversion and Conservation, National Research and Innovation Agency (BRIN), Indonesia. He received his bachelor's degree in electrical engineering from Udayana University in 2007 and his master's degree in energy management from Udayana University in 2012. He finished his Ph.D. in Electrical Engineering at National Taiwan University of Science and Technology (NTUST) in 2022. His research interests include electrical machines and energy management systems. He can be contacted at email: ketu003@brin.go.id.

Puji Widiyanto received his B.Eng. and M.Eng. degrees both in Mechanical Engineering, first in STT Mandala and later in Bandung Institute of Technology, Indonesia. Having focused his research on the structure, mechanical design, and manufacture of electrical machines, he is now working as a researcher at the Research Center for Energy Conversion and Conservation, the National Research and Innovation Agency (BRIN). Currently, he is conducting a project on a low-head hydropower system. He can be contacted at email: puji010@brin.go.id or pujiwidiyanto@gmail.com.